Geology, published online on 18 September 2012 as doi:10.1130/G33321.1

Unraveling the complexity of deep gas accumulations with three-dimensional multimodal CARS microscopy

Robert C. Burruss[1]*, Aaron D. Slepkov[4], Adrian F. Pegoraro[2,3], and Albert Stolow[2,3]*
[1]U.S. Geological Survey, Reston, Virginia 20192, USA
[2]Emerging Technologies Division, National Research Council, Ottawa, Ontario K1A 0R6, Canada
[3]Department of Physics, Queen's University, Kingston, Ontario K7L 3N6, Canada
[4]Department of Physics and Astronomy, Trent University, Peterborough, Ontario K9J 7B8, Canada

ABSTRACT

The origin of natural gas accumulations in thermally mature basins is poorly understood. Unraveling complex contributions from hydrocarbon cracking, mixing, redox alteration, and deeper sources requires analysis of gases trapped during specific periods of basin history. Fluid inclusions can provide such samples, but their unambiguous characterization is challenging. Here we show that three-dimensional (3-D) multimodal nonlinear optical microscopy of geologic materials allows mapping and molecular identification of trapped methane and water using coherent anti-Stokes Raman scattering, imaging of crystallographic features using second harmonic generation, and identification of higher hydrocarbons using two-photon excited fluorescence. Spatially resolved, molecule-specific characterization of fluid inclusions will improve models of natural gas generation, migration, and accumulation. We believe that these broadly applicable methods will potentially transform the characterization of geological materials.

INTRODUCTION

In deeply buried, thermally mature sedimentary basins, the geochemical processes that create accumulations of natural gas, including shale gas, are not well understood. Conventional models are based on late-stage cracking of kerogen and oil (Dieckmann et al., 2006; Hill et al., 2003), and laboratory simulations of these processes produce gases with stable isotopic compositions similar to gases associated with oil and condensate production. However, the isotopic compositions of nonassociated gases in thermally mature (vitrinite reflectance >2%) basins such as the Appalachian and Songliao Basins are reversed from normal patterns (Burruss and Laughrey, 2010; Dai et al., 2004), contradicting both the laboratory simulations and the predictions of *ab initio* models of isotopic fractionation (Tang et al., 2000). Isotopic reversals have been attributed to abiogenic, Fischer-Tropsch–type synthesis (Dai et al., 2004; Sherwood Lollar et al., 2002), raising the possibility of gas migration from deeper crustal or even upper mantle environments. Reversals can also be modeled by a combination of Rayleigh-type fractionation driven by oxidation-reduction reactions, mixing of gases associated with oil and condensate, and addition of methane from a deeper, higher-temperature source (Burruss and Laughrey, 2010). Determining the relative contributions of these processes to naturally occurring accumulations of gas will help resolve the current conflicts between nature and laboratory simulations, leading to more realistic models of the abundance and distribution of gas resources in deep basins. This requires analysis of gas samples directly tied to specific stages of the geologic history of thermally mature basins. Methane-rich hydrocarbon and aqueous fluid inclusions can provide such samples because they form in fracture-filling and diagenetic minerals during the extended history of gas generation, migration, and accumulation (Becker et al., 2010; Mullis et al., 1994; Parris et al., 2003). Unfortunately, inclusions frequently occur in complex, intersecting healed microfractures, often obscuring the less common primary inclusions (Parris et al., 2003), and making it difficult to determine the sequence of evolving temperature, pressure, and gas composition. Here we apply molecule-specific multimodal three-dimensional (3-D) nonlinear microscopy to provide chemically and spatially resolved imaging of assemblages of methane-rich fluid inclusions and associated crystallographic features, as well as in situ detection of higher hydrocarbons. These observations advance our ability to track gas generation and migration processes within deep basins.

METHODS AND SAMPLES

Our approach to molecule-specific 3-D imaging is based on a multimodal, nonlinear optical microscopy that includes coherent anti-Stokes Raman scattering (CARS), a nonlinear optical interaction sensitive to Raman vibrational resonances. CARS microscopy is a rapidly developing tool in biomedical science, predominantly applied to imaging lipid-rich structures via the C-H stretching vibration (Evans and Xie, 2008). Here we show that molecular imaging based on, for example, the C-H stretch applies equally to hydrocarbon gases such as CH_4 within fluid inclusions. Although CARS signals from low-density gases are generally weak, the density of CH_4 in inclusions can be high, on the order of 300 kg/m^3, yielding strong resonant CARS signals. Similar arguments apply to other trapped species such as H_2O, CO_2, and N_2.

In geosciences, CARS microscopy has significant advantages over spontaneous Raman scattering confocal microscopy. Our optimally chirped pulse implementation of CARS microscopy (Pegoraro et al., 2009) (described in the GSA Data Repository[1]) is based on femtosecond laser sources that generate additional signals such as two-photon excitation fluorescence (TPEF) and second harmonic generation (SHG) concurrent with the CARS image. Together, these modalities reveal in detail the distribution of hydrocarbons in gas-rich inclusions. The CARS signal is coherent, orders of magnitude more intense than spontaneous Raman scattering, and spectrally distinct from fluorescence, allowing separation of the C-H stretch spectrum of methane and higher hydrocarbons from the normally overwhelming autofluorescence background when petroleum liquids are present. Equally important, SHG reveals healed microfractures and other discontinuities in the quartz crystal lattice, as well as the 3-D distribution of fluid inclusions, providing new information on the history of trapping of inclusions. The intensity of each of these nonlinear signals permits short (2–8 µs) pixel dwell times, allowing rapid imaging of large 3-D fields of view (here 350 × 350 × 78 µm) within a few minutes. In scanning mode, CARS spectra are recorded from individual voxels within a user-defined region of interest (ROI), as shown in several figures. Spectra are displayed as averages of all voxels in the ROI.

We studied CH_4-rich fluid inclusions in samples from diagenetic, metamorphic, and igneous environments. The samples, described in Table DR1 (in the Data Repository), were chosen for proof-of-concept imaging of methane in a deep sedimentary basin and to demonstrate the potential for analysis of CH_4-rich fluids in deeper

*E-mails: burruss@usgs.gov; Albert.Stolow@nrc-cnrc.ca.

[1]GSA Data Repository item 2012310, Videos DR1–DR4, Table DR1, CARS methodology and image processing, and Figures DR1–DR3, is available online at www.geosociety.org/pubs/ft2012.htm, or on request from editing@geosociety.org or Documents Secretary, GSA, P.O. Box 9140, Boulder, CO 80301, USA.

crustal environments. Images were recorded using a modified inverted laser scanning confocal microscope (Olympus FV-300, ×40 water immersion objective). In our single-laser implementation, a femtosecond Ti:sapphire laser was used as both the pump beam and the source for subsequent Stokes beam generation in a photonic crystal fiber. For a pump wavelength of 800 nm, the CARS frequency is continuously and rapidly tuneable from 2100 to 4500 cm^{-1} (Pegoraro et al., 2009). CARS, SHG, and TPEF signals from the same focal volume were simultaneously collected using three separate photodetectors.

The CARS frequency range in the present study is narrower than the range recorded by conventional dispersive Raman spectrometers used in the geosciences, typically 200–4500 cm^{-1}. This range is not an intrinsic limitation. For example, we have imaged phosphate at 952 cm^{-1} and CO_2 at 1284 and 1388 cm^{-1}, simply by tuning the wavelength of the Ti:sapphire pump laser. (For discussion of differences in peak shape, peak position, and quantitation between CARS spectroscopy and conventional spontaneous Raman spectroscopy, see the Data Repository.)

3-D IMAGES AND SPECTRA

Imaging CH_4-rich inclusions in quartz from fracture-filling cements from the deep Appalachian Basin demonstrates the efficacy of our approach. In sample 1, a conventional bright-field transmitted-light image of CH_4-rich inclusions (Fig. 1A) shows a small number of inclusions in a single plane of focus, whereas the CARS image tuned to the ν_1 band of CH_4 (Fig. 1B) shows all CH_4-rich inclusions within a 350 × 350 × 78 µm scanning volume. A 3-D rendering (Video DR1) of the CARS image reveals the spatial distribution of the CH_4-rich inclusions within the field of view. Multimodal images of the largest inclusion (labeled i in Figs. 1A and 1B) are shown in Figures 1C–1F. Combined with the CARS spectrum (Fig. 1G), these images demonstrate the new information obtainable from multimodal CARS microscopy. The SHG response outlines the edge of the inclusion (Stoller et al., 2007) (Fig. 1C), the TPEF image shows the distribution of trace amounts of higher hydrocarbons on the inclusion wall (Fig. 1D), and the CARS signal confirms the presence of methane (Fig. 1E). The image of the combined signals (Fig. 1F) is highlighted with regions of interest from which CARS spectra (Fig. 1G) of the fluid and nonresonant background were recorded. The slight shift in CARS peak position (2905 cm^{-1}) from the known Raman peak position for dense CH_4 at 2914 ± 3 cm^{-1} (Lu et al., 2007) is due to partial interference of nonresonant background and the resonant CARS signal (discussed in the Data Repository). The discovery of fluorescence indicates the presence of higher-molecular-weight aromatic hydrocarbons within these gas-rich inclusions and opens new avenues of research on the origin of these compounds.

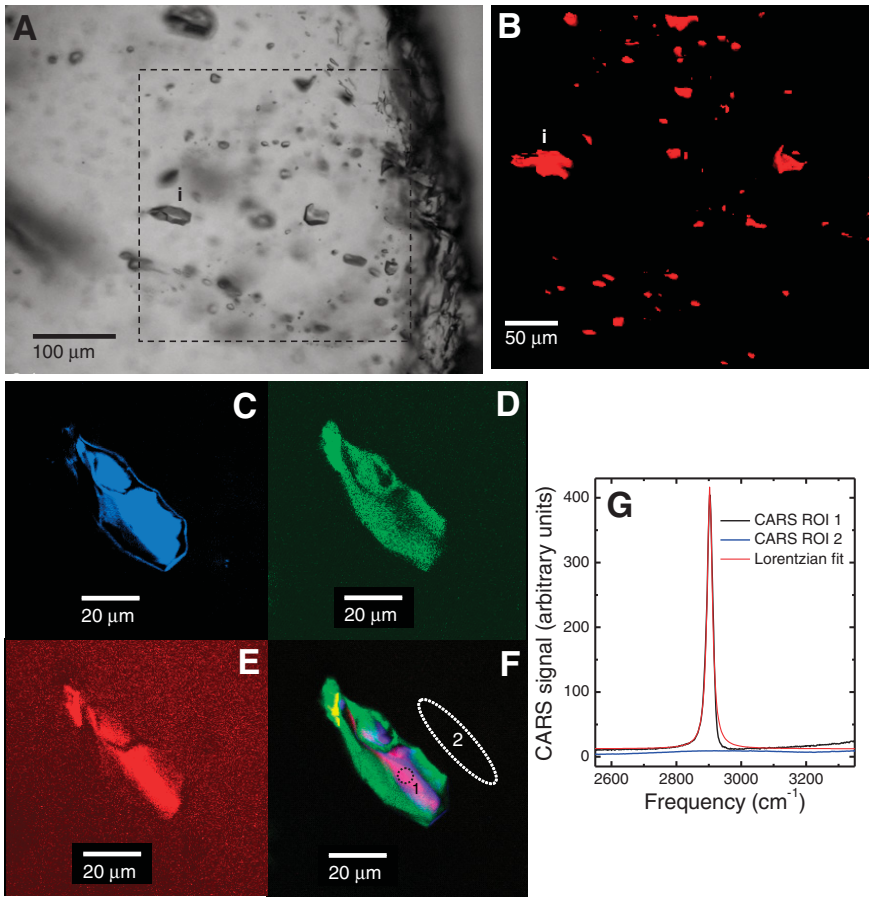

Figure 1. Multimodal images and coherent anti-Stokes Raman scattering (CARS) spectra of inclusions in sample 1. A: Bright-field, transmitted-light image of CH_4-rich fluid inclusions in quartz. Image is one plane of focus in conoscopic illumination. B: CARS image of CH_4-rich fluid inclusions in quartz. Image is flattened z-stack of all planes of focus showing all inclusions detected within 78-µm-thick field of view outlined in A. Three-dimensional rendering of B is shown in rotation in Video DR1 (see footnote 1). C–E: Single plane of focus in second harmonic generation, two-photon excitation fluorescence, and CARS detector channels, respectively, from the largest inclusion (labeled i in A and B). F: All three channels overlaid with regions of interest (ROI: 1, 2) from which spectra for inclusion and non-resonant background in quartz host were recorded. G: Display of spectra from ROI in F.

In another field of view within sample 1, small inclusions appear as an array that dips steeply into the plane of the section. Combined CARS and SHG images reveal that this set of inclusions is clearly associated with a healed microfracture imaged by the SHG response to the crystallographic lattice mismatch (Ríos et al., 2001) across the microfracture (Fig. 2). Such microfractures are part of the structural fabric of the rock and reflect the history of deformation and associated fluid flow. Rotation of the multimodal 3-D image (Video DR2) provides unprecedented visualization of the association of inclusions with a distinct generation of microfracture.

Sample 2 contains both CH_4- and H_2O-rich inclusions (Fig. 3) that were trapped within quartz during burial deeper within the Appalachian

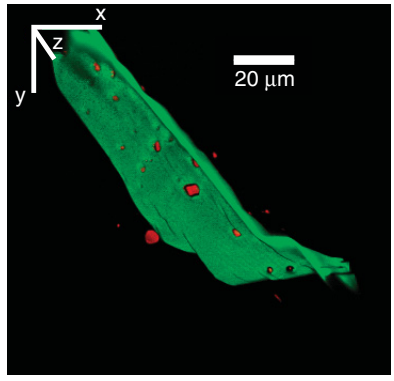

Figure 2. First frame of three-dimensional (3-D) animation (Video DR2 [see footnote 1]) of CH_4-rich inclusions (imaged by coherent anti-Stokes Raman scattering; red) along or adjacent to healed microfracture (imaged by second harmonic generation; green). Images of crystallographic discontinuities in 3-D provide unprecedented ability to define relationship of fluid inclusions to individual microfractures.

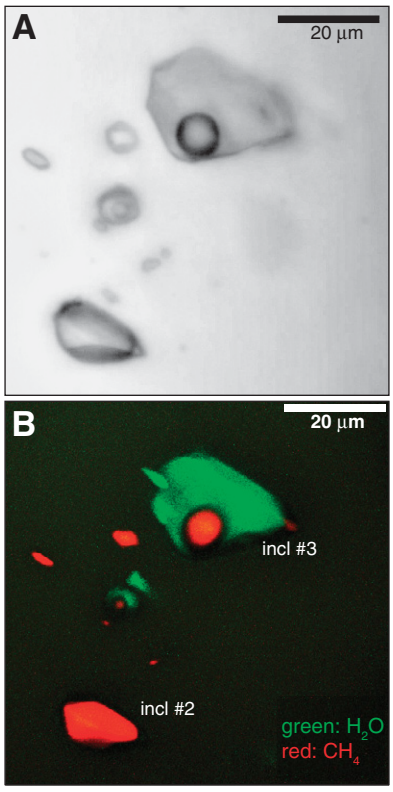

Figure 3. A: Bright-field transmitted light image of collapsed z-stack of field of view with one-phase CH_4-rich inclusions and two-phase water-methane inclusions. B: Coherent anti-Stokes Raman scattering (CARS) image of A. Methane is red and water is green. In this field of view we can identify CH_4-rich inclusions (incl 2) and methane in vapor bubble of two-phase aqueous inclusions (incl 3). Small volume of water visible in A in tip of inclusion 2 produced weak CARS signal that was lost during signal processing. Three-dimensional rendering of B is shown in rotation in Video DR3 (see footnote 1), and CARS spectra of inclusion 2 and aqueous phase of inclusion 3 are shown in Figure DR1.

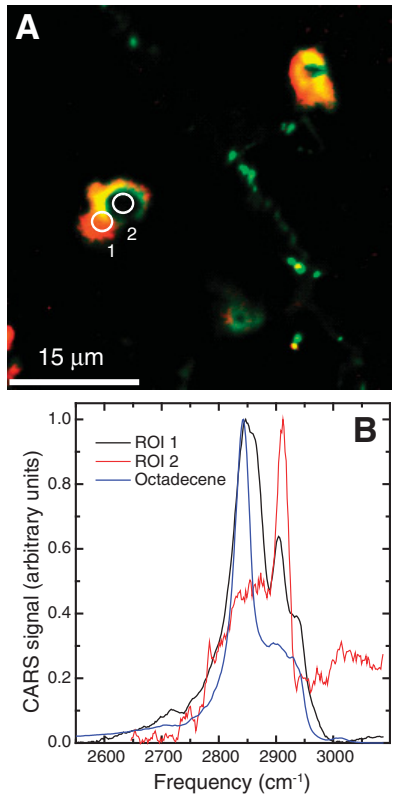

Figure 4. A: Multimodal image of fluorescent crude oil fluid inclusions in calcite (sample 5). Large inclusions have dark and relatively nonfluorescent vapor bubbles. B: Coherent anti-Stokes Raman scattering (CARS) spectra (at 2850 cm^{-1}) of inclusions in A. Regions of interest (ROI) labeled 1 and 2 are crude oil liquid and vapor bubble, respectively, with spectra displayed. Spectrum of liquid (ROI 1, black trace) shows peak for CH_4 dissolved in liquid with larger peak for C-H stretching of liquid hydrocarbons. Red trace (ROI 2) shows strong peak for methane above broader band for C-H stretch of higher hydrocarbons in vapor. Spectrum of pure octadecene is shown in blue for comparison.

Basin than those of sample 1. The CARS image created by the vibrational contrast from methane at 2905 cm^{-1} and water at 3230 cm^{-1} (Fig. DR1) demonstrates the identification of chemically distinct phases within individual inclusions. The 3-D visualization (Video DR3) shows a close spatial association of single-phase CH_4-rich inclusions with two-phase aqueous inclusions containing a CH_4-rich vapor bubble. The ability to broadly identify CH_4-rich vapor bubbles in aqueous inclusions is an important advance in the characterization of inclusion-bearing samples, allowing us to clearly distinguish different assemblages of aqueous inclusions based on the gas content of the vapor bubble.

Identifying the location and type of hydrocarbons in deep crustal environments is challenging. To test the ability of our technique to do so, we examined two samples (Figs. DR2 and DR3) from high-temperature metamorphic (sample 3) and igneous (sample 4) environments that are known to contain CH_4-rich inclusions (Burruss, 1977; Vanko and Stakes, 1991). In addition to the CH_4 CARS response, we spectroscopically identified N_2 (Fig. DR2) within CH_4-rich inclusions in sample 3. We observed fluorescence signals (TPEF) from CH_4-rich inclusions in both samples (Figs. DR2 and DR3), indicating the presence of aromatic hydrocarbons. Fluorescence is not detectable within these inclusions using conventional wide-field fluorescence microscopy (Burruss, 2003a). Although trace quantities of solvent-extractable high-molecular-weight hydrocarbons from igneous and metamorphic rocks were reported (Price and DeWitt, 2001), their significance and origin remain controversial. Our nondestructive confirmation of higher hydrocarbons inside fluid inclusions within high-temperature rocks will permit screening of inclusion-bearing grains for analysis by ultralow background crush-leach and gas chromatography–mass spectrometry methods (George et al., 1997). This will allow detailed characterization of hydrocarbons that are unambiguously indigenous to high-temperature rock samples.

In conventional models of natural gas formation, the time of late-stage cracking and the transition from gas plus liquids to nonassociated gas during basin evolution is not well constrained. Fluid inclusion measurements combined with thermochronology identify short intervals of gas generation (Parris et al., 2003), helping to determine the transition from hydrocarbon liquids plus gas to gas during basin evolution. Unfortunately, composition and density analysis of gas-liquid hydrocarbon inclusions using conventional confocal Raman spectroscopy is, in practice, unfeasible (Burruss, 2003b) because fluorescence emission from higher hydrocarbons within the liquid overwhelms any spontaneous Raman scattering (McCreery, 2000) from the liquid or the gas phase. CARS microscopy overcomes this limitation in two ways. First, the signal from the nonlinear CARS process is several orders of magnitude more intense than that of spontaneous Raman scattering, and second, the CARS response is a coherent forward-propagating signal (Evans and Xie, 2008), facilitating its separation from the isotropic fluorescence emission.

We successfully imaged two-phase gas-liquid hydrocarbon inclusions in calcite with TPEF and CARS (sample 5, Fig. 4). Despite a strong TPEF signal (Fig. 4A), the CARS signal is distinctly separated from the fluorescence, allowing spectroscopy of C-H stretching bands from CH_4 and higher hydrocarbons in both the vapor and liquid phases (Fig. 4B). This is a major advance in the analysis of gases in crude oil and condensate inclusions because the position of the CH_4 ν_1 peak is pressure sensitive (Lu et al., 2007). CARS microspectroscopy will allow estimation of methane mole fractions and internal pressures within gas and liquid hydrocarbon inclusions, information that is required by pressure-temperature-volume models (Thiéry et al., 2002) for estimating temperatures and pressures in the deep basins during hydrocarbon liquid to gas cracking.

CONCLUSIONS

Our results clearly demonstrate that multimodal nonlinear optical microscopy with simultaneous CARS, SHG, and TPEF imaging and spectroscopy provides major advances in identification and characterization of assemblages of methane-rich fluid inclusions. The unique ability of SHG to simultaneously generate 3-D images of inclusion volumes, microfractures, grain boundaries, and other crystallographic discontinuities provides unprecedented characterization of the trapping history of fluids within

inclusions. These advances, coupled with identification of methane-rich inclusions containing traces of higher hydrocarbons in metamorphic and igneous rocks, present new approaches to identifying distinct generations of CH_4-rich gases, including deep crustal gases, that may create natural gas resources.

Nonlinear optical imaging and spectroscopy of fluid inclusions is likely to be only one of many applications in the geosciences. Nonlinear optical techniques are sensitive to interfacial processes of environmental and biogeochemical importance (Geiger, 2009), including biofilms (Hu et al., 2005). SHG was discovered in quartz (Franken et al., 1961) and applied to clay minerals (Newnham et al., 1977); this suggests a broad range of possible mineralogical applications. The technology of multimodal CARS imaging and spectroscopy is evolving rapidly, with improvements in imaging speed, spectral range, spectral resolution, and quantitation. We believe that multimodal nonlinear optical microscopy has the potential to revolutionize our ability to image and analyze geological samples.

ACKNOWLEDGMENTS

We thank the Natural Sciences and Engineering Research Council of Canada for financial support. Burruss acknowledges support of the Eastern Energy Resources Science Center Director, James L. Coleman (U.S. Geological Survey). Mark Evans and David Vanko contributed samples. We thank Robert Bodnar (Virginia Tech) and Dennis Klug (National Research Council of Canada, NRC) for their insight and encouragement, Marcus Cicerone (National Institute of Standards and Technology) for the Raman retrieval algorithm, Andrew Ridsdale and Douglas Moffatt (NRC) for fruitful discussions and assistance in data processing, and Julien Bourdet for a thorough review. Use of commercial trade names is for information purposes only and does not constitute endorsement by the United States or Canadian governments.

REFERENCES CITED

Becker, S.P., Eichhubl, P., Laubach, S.E., Reed, R.M., Lander, R.H., and Bodnar, R.J., 2010, A 48 m.y. history of fracture opening, temperature, and fluid pressure: Cretaceous Travis Peak Formation, East Texas basin: Geological Society of America Bulletin, v. 122, p. 1081–1093, doi:10.1130/B30067.1.

Burruss, R.C., 1977, Analysis of fluid inclusions in graphitic metamorphic rocks from Bryant Pond, Maine, and Khtada Lake, British Columbia: Thermodynamic basis and geologic interpretation of observed fluid compositions and molar volumes [Ph.D. thesis]: Princeton, New Jersey, Princeton University, 156 p.

Burruss, R.C., 2003a, Petroleum fluid inclusions, an introduction, *in* Samson, I.M., et al., eds., Fluid inclusions: Analysis and interpretation: Mineralogical Association of Canada Short Course Series, v. 32, p. 159–174.

Burruss, R.C., 2003b, Raman spectroscopy of fluid inclusions, *in* Samson, I.M., et al., eds., Fluid inclusions: Analysis and interpretation: Mineralogical Association of Canada Short Course Series, v. 32, p. 279–290.

Burruss, R.C., and Laughrey, C.D., 2010, Carbon and hydrogen isotopic reversals in deep basin gas: Evidence for limits to the stability of hydrocarbons: Organic Geochemistry, v. 41, p. 1285–1296, doi:10.1016/j.orggeochem.2010.09.008.

Dai, J., Xia, X., Qin, S., and Zhao, J., 2004, Origins of partially reversed alkane $\delta^{13}C$ values for biogenic gases in China: Organic Geochemistry, v. 35, p. 405–411, doi:10.1016/j.orggeochem.2004.01.006.

Dieckmann, V., Ondrak, R., Cramer, B., and Horsfield, B., 2006, Deep basin gas: New insights from kinetic modelling and isotopic fractionation in deep-formed gas precursors: Marine and Petroleum Geology, v. 23, p. 183–199, doi:10.1016/j.marpetgeo.2005.08.002.

Evans, C.L., and Xie, X.S., 2008, Coherent anti-Stokes Raman scattering microscopy: Chemical imaging for biology and medicine: Annual Reviews of Analytical Chemistry, v. 1, p. 883–909, doi:10.1146/annurev.anchem.1.031207.112754.

Franken, P.A., Hill, A.E., Peters, C.W., and Weinreich, G., 1961, Generation of optical harmonics: Physical Review Letters, v. 7, p. 118–119, doi:10.1103/PhysRevLett.7.118.

Geiger, F.M., 2009, Second harmonic generation, sum frequency generation and χ^3: Dissecting environmental interfaces with a nonlinear optical Swiss army knife: Annual Review of Physical Chemistry, v. 60, p. 61–83, doi:10.1146/annurev.physchem.59.032607.093651.

George, S.C., Krieger, F.W., Eadington, P.J., Quezada, R.A., Greenwood, P.F., Eisenberg, L.I., Hamilton, P.J., and Wilson, M.A., 1997, Geochemical comparison of oil-bearing fluid inclusions and produced oil from the Toro sandstone, Papua New Guinea: Organic Geochemistry, v. 26, p. 155–173, doi:10.1016/S0146-6380(97)00004-1.

Hill, R.J., Tang, Y., and Kaplan, I.R., 2003, Insights into oil cracking based on laboratory experiments: Organic Geochemistry, v. 34, p. 1651–1672, doi:10.1016/S0146-6380(03)00173-6.

Hu, Z., Hidalgo, G., Houston, P.L., Hay, A.G., Shuler, M.L., Abruna, H.D., Ghiorse, W.C., and Lion, L.W., 2005, Determination of spatial distributions of zinc and active biomass in microbial biofilms by two-photon laser scanning microscopy: Applied and Environmental Microbiology, v. 71, p. 4014–4021, doi:10.1128/AEM.71.7.4014-4021.2005.

Lu, W., Chou, I.-M., Burruss, R.C., and Song, Y., 2007, A unified equation for calculating methane vapor pressures in the CH_4-H_2O system with measured Raman shifts: Geochimica et Cosmochimica Acta, v. 71, p. 3969–3978, doi:10.1016/j.gca.2007.06.004.

McCreery, 2000, Raman spectroscopy for chemical analysis: New York, Wiley-Interscience, 420 p.

Mullis, J., Dubessy, J., Poty, B., and O'Neil, J., 1994, Fluid regimes during late stages of a continental collision: Physical, chemical, and stable isotope measurements of fluid inclusions in fissure quartz from a geotraverse through the Central Alps, Switzerland: Geochimica et Cosmochimica Acta, v. 58, p. 2239–2267, doi:10.1016/0016-7037(94)90008-6.

Newnham, R.E., Kramer, J.J., Schulze, W.A., and Brindley, G.W., 1977, Optical second harmonic signals from clay minerals: Physics and Chemistry of Minerals, v. 1, p. 379–384, doi:10.1007/BF00308847.

Parris, T.M., Burruss, R.C., and O'Sullivan, P.B., 2003, Deformation and timing of gas generation and migration in the eastern Brooks Range foothills, Arctic National Wildlife Refuge, Alaska: American Association of Petroleum Geologists Bulletin, v. 87, p. 1823–1846, doi:10.1306/07100301111.

Pegoraro, A.F., Ridsdale, A., Moffat, D.J., Jia, Y., Pezacki, J.P., and Stolow, A., 2009, Optimally chirped multimodal CARS microscopy based on a single Ti:sapphire oscillator: Optics Express, v. 17, p. 2984–2996, doi:10.1364/OE.17.002984.

Price, L.C., and DeWitt, E., 2001, Evidence and characteristics of hydrolytic disproportionation of organic matter during metasomatic processes: Geochimica et Cosmochimica Acta, v. 65, p. 3791–3826, doi:10.1016/S0016-7037(01)00762-1.

Ríos, S., Salje, E.K.H., and Redfern, S.A.T., 2001, Nanoquartz vs. macroquartz: A study of the alpha-beta phase transition: European Physical Journal B, v. 20, p. 75–83, doi:10.1007/s100510170286.

Sherwood Lollar, B., Westgate, T.D., Ward, J.A., Slater, G.F., and Lacrampe-Couloume, G., 2002, Abiogenic formation of alkanes in the Earth's crust as a minor source for global hydrocarbon reservoirs: Nature, v. 416, no. 6880, p. 522–524, doi:10.1038/416522a.

Stoller, P., Kruger, Y., Ricka, J., and Frenz, M., 2007, Femtosecond lasers in fluid inclusion analysis: Three-dimensional imaging and determination of inclusion volume in quartz using second harmonic generation microscopy: Earth and Planetary Science Letters, v. 253, p. 359–368, doi:10.1016/j.epsl.2006.10.037.

Tang, Y., Perry, J.K., Jenden, P.D., and Schoell, M., 2000, Mathematical modeling of stable carbon isotope ratios in natural gases: Geochimica et Cosmochimica Acta, v. 64, p. 2673–2687, doi:10.1016/S0016-7037(00)00377-X.

Thiéry, R., Pironon, J., Walgenwitz, F., and Montel, F., 2002, Individual characterization of petroleum fluid inclusions (composition and *P-T* trapping conditions) by microthermometry and confocal laser scanning microscopy: Inferences from applied thermodynamics of oils: Marine and Petroleum Geology, v. 19, p. 847–859, doi:10.1016/S0264-8172(02)00110-1.

Vanko, D.A., and Stakes, D.S., 1991, Fluids in oceanic layer 3: Evidence from veined rocks, Hole 735B, southwest Indian Ridge, *in* Von Herzen, R.P., et al., Proceedings of the Ocean Drilling Program, Scientific results, Volume 118: College Station, Texas, Ocean Drilling Program, p. 181–215, doi:10.2973/odp.proc.sr.118.121.1991.

Manuscript received 16 February 2012
Revised manuscript received 30 April 2012
Manuscript accepted 27 May 2012

Printed in USA